 doi:10.20944/preprints201812.0215.v1

Combined Magnesia, Ceria and Nickel catalyst supported over γ-Alumina Doped with Titania for Dry Reforming of Methane

Ahmed Sadeq Al-Fatesh [1,*], Samsudeen Olajide Kasim [1], Ahmed Aidid Ibrahim [1], Anis Hamza Fakeeha [1], Ahmed Elhag Abasaeed [1], Rasheed Arasheed [2], Rawan Ashamari [2], Abdulaziz Bagabas [2,*]

[1] Chemical Engineering Department, College of Engineering, King Saud University, P.O. Box 800, Riyadh 11421, Saudi Arabia; aalfatesh@ksu.edu.sa (A.S.A.-F.); sofkolajide2@gmail.com (S.O.K.); aidid@ksu.edu.sa (A.A.I.); anishf@ksu.edu.sa (A.H.F.); abasaeed@ksu.edu.sa (A.E.A)

[2] National Petrochemical Technology Center (NPTC), Materials Science Research Institute (MSRI), King Abdulaziz City for Science and Technology, P.O. Box 6086, Riyadh 11442, Saudi Arabia; rrisheed@kacst.edu.sa (R.Ar.); ralshammary@kacst.edu.sa (R. As.); abagabas@hotmail.com (A.B.)

* Correspondence: aalfatesh@ksu.edu.sa (A.S.A.-F), abagabas@hotmail.com (A.B); Tel.: +966-11-467-6859, +966-11-481-3790

Abstract: This study investigated dry reforming of methane with combined catalysts supported on γ-Al_2O_3 support doped with 3.0 wt. % TiO_2. The physicochemical properties of all the catalysts were determined by inductively-coupled plasma/mass spectrometry metal analysis, nitrogen physisorption, X-ray diffraction, temperature programmed reduction/desorption, thermogravimetric analysis, and scanning electron microscopy. The addition of CeO_2 and MgO to Ni strengthened the interaction between the Ni and the support. The catalytic activity results indicated that the CeO_2 and MgO addition to Ni did not do much in retarding carbon deposition, but they improved the activity of the catalysts. Among the tested catalysts, it was found that the catalyst with the composition of 5.0 wt % NiO-10.0 wt % CeO_2/3.0 wt %TiO_2-γ-Al_2O_3 resulted in the highest CH_4 and CO_2 conversion with H_2/CO mole ratio close to unity. The optimum reaction conditions in terms of reactant conversion and H_2/CO mole ratio were achieved by varying space velocity and CO_2/CH_4 mole ratio.

Keywords: CH_4, CeO_2, Dry reforming, MgO, Ni, TiO_2

1. Introduction

The global warming has become an alarming issue. The emissions of greenhouse gases of carbon dioxide and methane (CO_2 and CH_4) contribute actively to this problem. Methods of transforming these two gases into useful products are worth from the prospect of the environmental safety and the economic point of view of generating value-added fuels and chemicals [1-3]. In this context, numerous reforming reactions of CH_4 have been employed using several oxidants such H_2O, CO_2 and O_2 for the production of hydrogen or synthesis gas (syngas; hydrogen and carbon monoxide mixture) with a H_2:CO molar ratio of one through processes such as steam reforming of methane, auto thermal reforming, tri-reforming of methane, etc. [7-11]. The CO_2 reforming of methane process, known as dry reforming of CH_4 (DRM), has attracted the

Preprints (www.preprints.org) | NOT PEER-REVIEWED | Posted: 18 December 2018 doi:10.20944/preprints201812.0215.v1

investigators because it mitigates the emission of CH_4 and CO_2, transforms them into synthesis gas, the starting material in the Fischer-Tropsch process to generate hydrocarbons and oxygenates, and generates clean energy through the combustion of hydrogen [12]. CH_4 is the chief component of natural gas and biogas with the total composition of 80-90%. Therefore, it is cost-effective feedstock for syngas production. The primary reaction that governs the process is as follows:

$$CH_4 + CO_2 \rightarrow 2H_2 + 2CO \qquad \Delta H_{298} = +247\ kJmol^{-1} \qquad [1]$$

The reaction is immensely endothermic and needs to be operated at high temperature for the achievement of acceptable conversions. The active elements in the catalyst of the CO_2 reforming of methane include both noble metals such as Ru, Rh, or Pt, and first row transition metals like Ni, Fe, and Co. Although noble metals display high activity and stability, their limited availability and high price have made them inappropriate for industrial use [13, 14]. On the other hand, the first row transition metals are cheaper and possess similar activity, but their stability is hampered by carbon deposition and particle sintering [15-18]. Therefore, the development of Ni-based catalysts with high activity and resistance to the deactivation due to the carbon formations and metal sintering is essential for DRM. Many efforts have been carried out to develop catalysts that possess high activity and stability. The catalytic performance can be influenced by many factors such as the active metal and support type and texture. The support enhances the catalyst selectivity, activity and stability by increasing the surface area and the active metal dispersion [19]. Alumina support has high specific surface area and promotes active metal dispersion on its surface which results in high catalytic activity. But, Ni deactivates fast due to sintering, coke deposition, and formation of surface nickel aluminate phase that influences the entire dynamics of CO_2 reforming process. To increase the catalytic performance of nickel/γ-alumina, various parameters can be incorporated in the catalyst.

Pure Titania (TiO_2) is characterized by low specific surface area, poor mechanical strength, and phase transformation (anatase to rutile) at high temperatures, and thus, it does not suit for high temperature reactions [20]. Previous studies exhibited that introducing thermally stable second metal oxide like silica (SiO_2) can stabilize the degradation of the textural properties of the TiO_2 and can be employed as support [21, 22]. Incorporation of TiO_2 in the alumina support improves the dispersion of metal on the support, lowers the sintering, upgrades the stability to heat, in addition, enhances the capacity to store oxygen which assists in gasifying the carbon that was produced in the course of the reforming reaction [23]. Tauster et al investigated the effects of modification of the support on the oxidation state of ruthenium (Ru) and the catalytic performance of Ru/TiO_2 catalysts under conditions of partial oxidation of methane to synthesis gas. It was found that doping of TiO_2 with small amounts of W^{6+} cations favored oxygen adsorption on Ru under reaction conditions, and thus, it resulted in stabilization of a fraction of the catalyst in its oxidized forms [25]. On the other hand, the active Ni metal component has been improved by the addition of metal oxide promoters. For instance, Shamskar et al. investigated the addition of ceria (CeO_2), lanthana (La_2O_3), and zirconia (ZrO_2) to Ni/Al_2O_3 catalyst used for DRM and found that ceria-promoted catalyst reduced the carbon formation [25]. $Ni\text{-}MgO\text{-}Al_2O_3$ catalysts were used for steam reforming of methane by Jang et al. [26]. Al-Fatesh et al studied the promotional effect of ceria in the catalytic DRM and found that the Ni doping with ceria resulted in an excellent activity and less coke formation [27]. The magnesia (MgO) promoter enhanced the CH_4 conversion and mitigated the effect of the potassium poisoning of the Ni-based catalyst. The MgO promoter is beneficial in suppressing carbon formation.

In the present work, supported combination of Mg, Ce and Ni catalysts have been developed to retain high activity and stability while reducing the formation of coke during the DRM. The

Preprints (www.preprints.org) | NOT PEER-REVIEWED | Posted: 18 December 2018 doi:10.20944/preprints201812.0215.v1

effect of using MgO and CeO_2 as separate and combined promoters, for 5.0 wt % NiO supported over γ-Al_2O_3 doped with 3.0 wt % TiO_2 was studied. Different techniques were employed to characterize the various prepared catalyst systems to perceive the observed catalytic performance and the impact of each modifier.

2. Results and Discussion

2.1. Structure and Morphology

The XRD patterns of all the fresh catalysts are displayed in Figure 1. All the patterns consisted of various metal oxides, where the presence metal oxide phases depended on the added components used to prepare the catalysts. Three metal oxides existed in all catalysts, where these metal oxides were the component of the support: cubic gamma-aluminum oxide, γ-$(Al_2O_3)_{1.333}$ (PDF 01-075-0921), cubic synthesized honguiite titanium oxide, $(TiO_{0.8})_{0.913}$ (PDF 01-085-1380), and aluminum silicate, $Al_{0.5}Si_{0.75}O_{2.25}$ (PDF 00-037-1460). On the other hand, rhombohedral nickel oxide, NiO (PDF 00-044-1159) was found in Ti-CAT-I, Ti-CAT-II, Ti-CAT-III, and Ti-CAT-V. However, when magnesium was added, cubic magnesium nickel oxide, $MgNiO_2$ (PDF 00-024-0712) formed. Cubic synthesized cerianite (Ce) (ceria), CeO_2 (PDF 00-034-0394), was detected in Ti-CAT-I, Ti-CAT-II, Ti-CAT-IV, and Ti-CAT-VI. Addition of magnesium influenced strongly the interaction of cerium with the other components of the catalyst, where monoclinic magnesium cerium oxide, $MgCeO_3$ (PDF 00-004-0641), and cubic magnesium cerium titanium oxide, Mg_2CeTiO_6 (PDF 00-058-0550) existed in Ti-CAT-I and Ti-CAT-IV. Cubic periclase magnesium oxide, MgO (PDF 01-071-1176) was detected in Ti-CAT-I, Ti-CAT-III, and Ti-CAT-IV. Therefore, XRD was a powerful technique to explore how each catalyst component affect other component through the formation of mixed metal oxides.

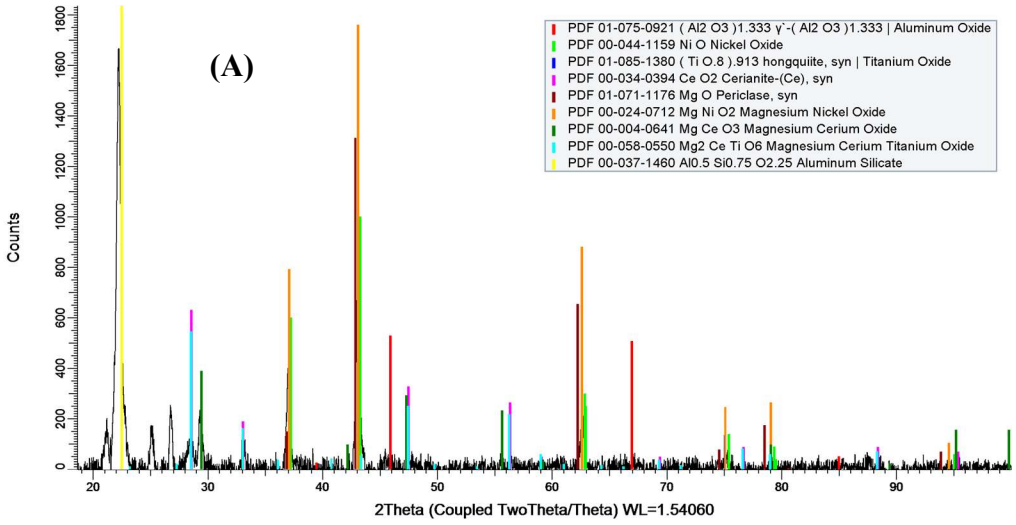

Preprints (www.preprints.org) | NOT PEER-REVIEWED | Posted: 18 December 2018 doi:10.20944/preprints201812.0215.v1

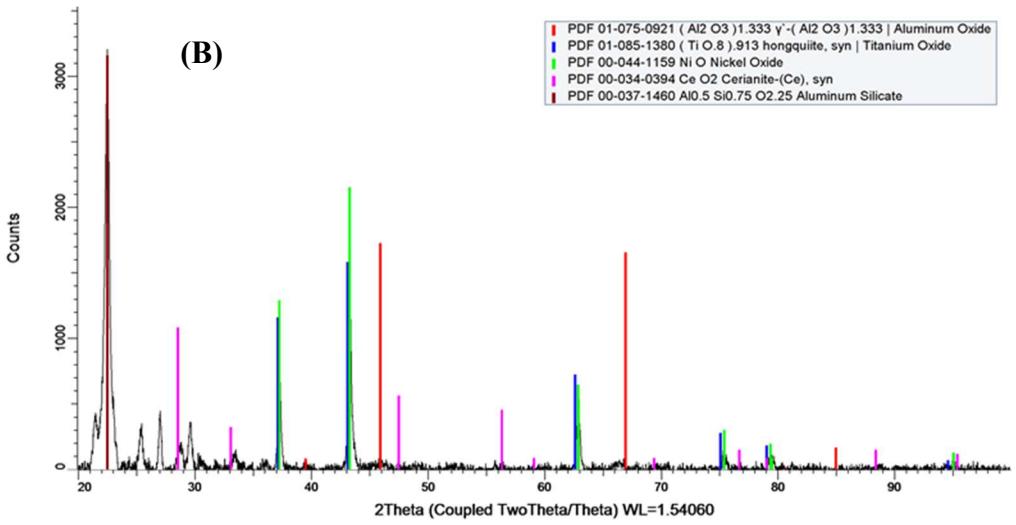

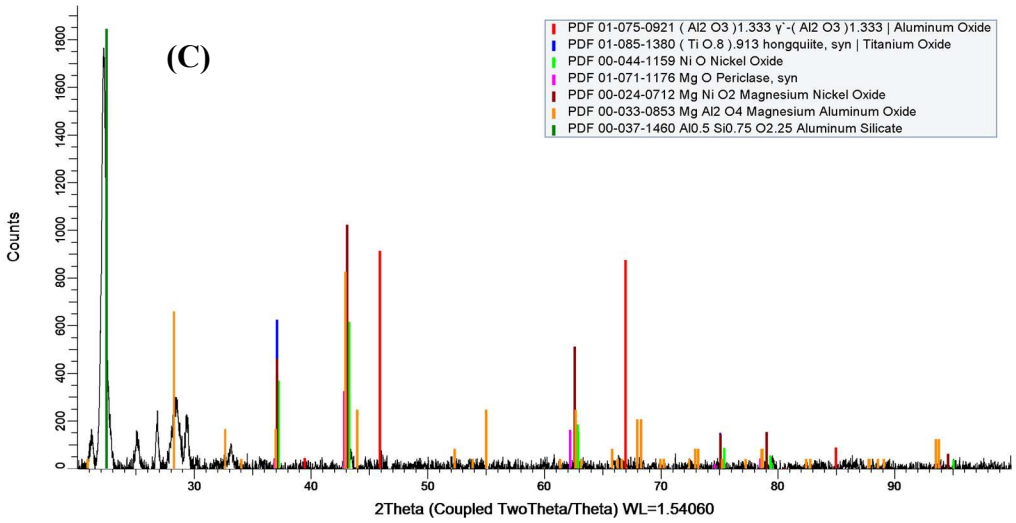

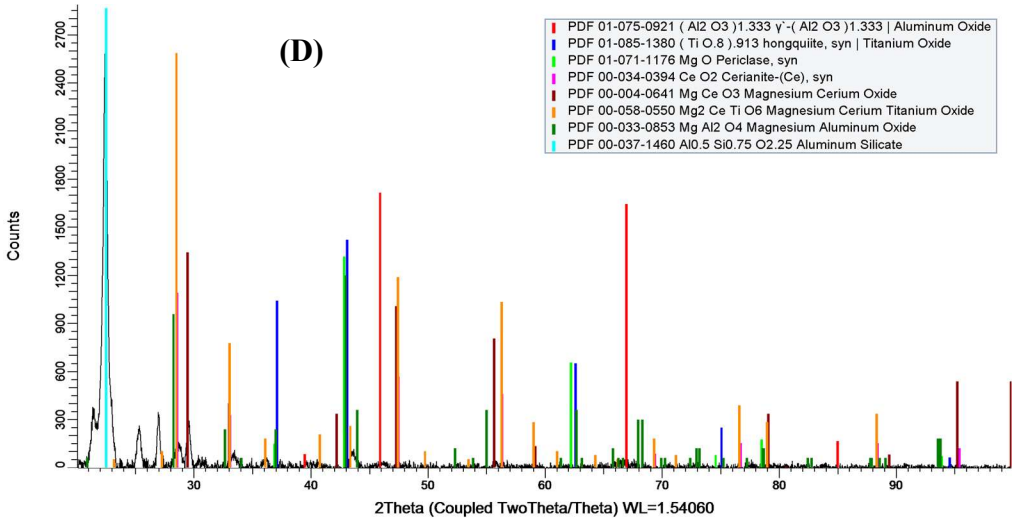

Preprints (www.preprints.org) | NOT PEER-REVIEWED | Posted: 18 December 2018 doi:10.20944/preprints201812.0215.v1

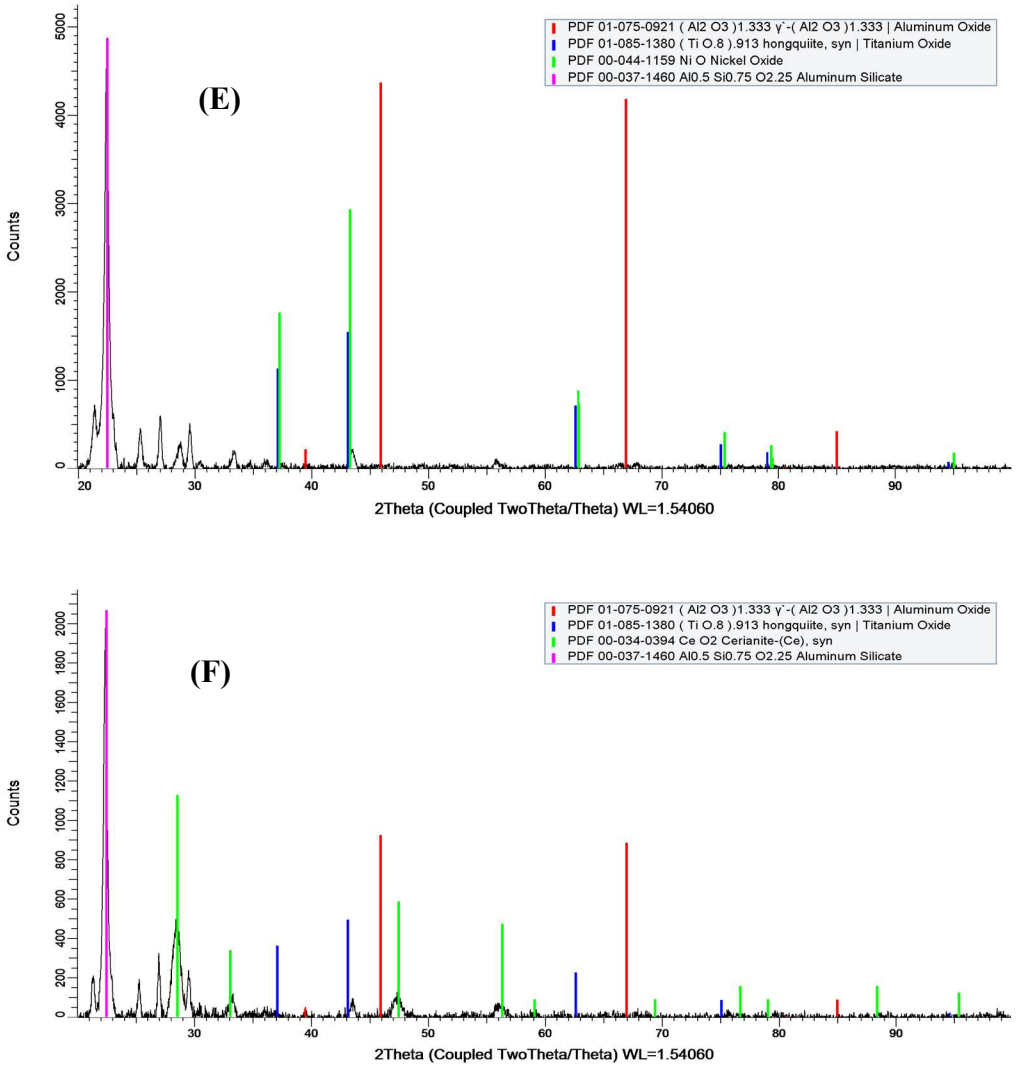

Figure 1. XRD patterns of fresh catalysts: (A) Ti-CAT-I, (B) Ti-CAT-II, (C) Ti-CAT-III, (D) Ti-CAT-IV, (E) Ti-CAT-V, and (F) Ti-CAT-VI.

Both fresh and spent catalysts had their morphology explored by SEM technique. Figure 2 shows the SEM micrographs for the best two catalysts: Ti-CAT-I and Ti-CAT-II. Similar morphology, based on agglomerated, spherical nanoparticles, was detected for both fresh catalysts [Figure 2 (A) and (B)]. Such observation was expected because both catalysts were synthesized by identical preparation procedure and had similar component with the exception that Ti-CAT-II had no magnesium in its matrix.

The morphology of the spent catalysts was similar to that one of the fresh samples except the presence of carbon nanotubes (CNTs) on the surface of the spent catalysts [Figure 2 (C) and (D)]. Detection of CNTs on the surface of the spent catalyst confirms the results of TGA of spent catalysts. The presence of CNTs on the surface of the spent catalysts could be attributed to Boudouard reaction, which in turn, would be responsible for reducing the catalytic performance.

Preprints (www.preprints.org) | NOT PEER-REVIEWED | Posted: 18 December 2018 doi:10.20944/preprints201812.0215.v1

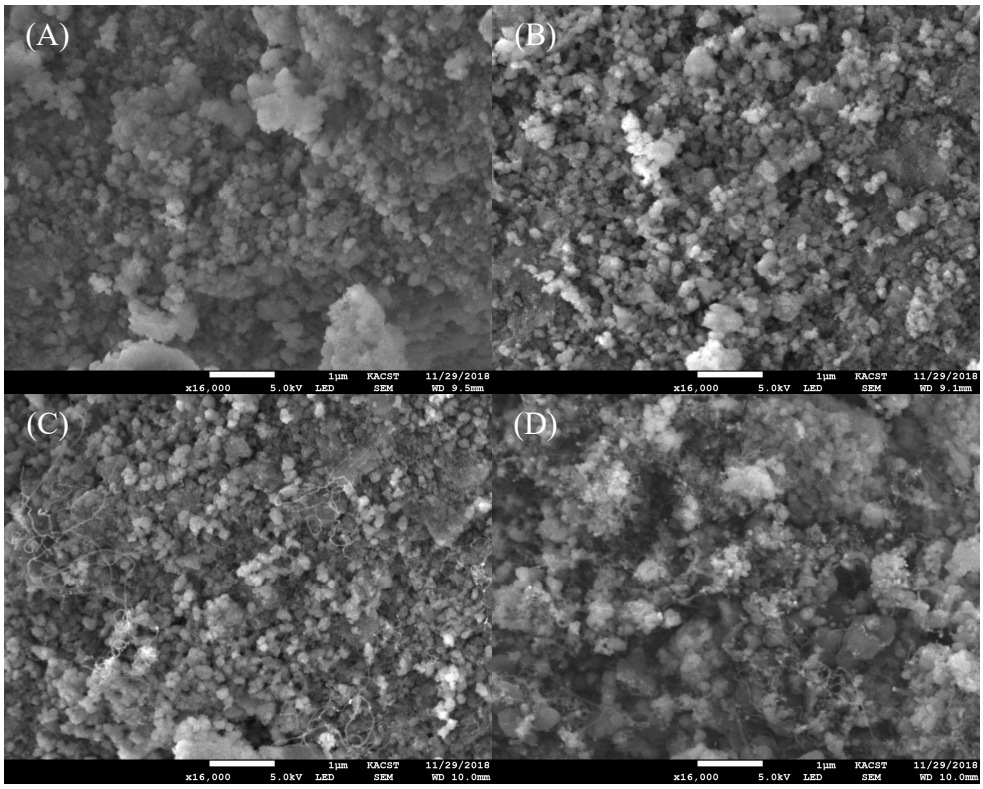

Figure 2. SEM micrographs for fresh catalysts (A) Ti-CAT-I, (B) Ti-CAT-II, and spent catalysts (C) Ti-CAT-I, (D) Ti-CAT-II.

2.2. Inductively Coupled Plasma Mass Spectroscopy (ICP-MS)

ICP-MS analysis was carried out to quantify the metallic components as metal oxides for the best two catalysts. The results are shown in the two tables below.

Table 1 summarizes the results of ICP analysis of the metallic components in the prepared catalysts and compares it with the theoretical values. The experimental results were found to be in excellent agreement with the nominal values. Therefore, ICP analysis confirmed the success of our preparation procedure for our targeted catalysts.

Preprints (www.preprints.org) | NOT PEER-REVIEWED | Posted: 18 December 2018 doi:10.20944/preprints201812.0215.v1

Table 1a. ICP metal oxide microanalysis of Ti-CAT-I.

Catalyst	**Ti-CAT-I**					
Component	**NiO**	**CeO_2**	**MgO**	**TiO_2**	**SiO_2**	**Al_2O_3**
Theoretical, wt/wt %	5.00	10.00	1.00	3.00	2.00	79.00
Experimental, wt/wt %	5.21	9.91	1.02	2.86	1.93	78.05

Table 1b. ICP metal oxide microanalysis of Ti-CAT-II.

Catalyst	**Ti-CAT-II**					
Component	**NiO**	**CeO_2**	**MgO**	**TiO_2**	**SiO_2**	**Al_2O_3**
Theoretical, wt/wt %	5.00	10.00	0.00	3.00	2.00	79.00
Experimental, wt/wt %	4.98	10.11	0.00	2.92	2.07	81.03

2.3. Temperature Programmed Desorption (CO_2-TPD)

CO_2-TPD experiment was performed to study the basicity of the catalysts. The obtained results are shown in figure 3.

Catalyst's basicity has paramount influence on the catalytic performance in DRM due to the acidic nature of CO_2. Thus, strong basic sites can enhance the catalytic activity and increases the chemisorption and reaction of reacting gases [28]. Basic sites' distribution on the catalyst, i.e. weak, intermediate, strong, and very strong, correspond to peaks in the temperature ranges of 20–150°C, 150–300°C, 300–450°C, and >450°C, respectively, in CO_2-TPD profile [29, 30].

From figure 3, all the catalysts except 5.0 wt % NiO/3.0 wt % TiO_2-γ-Al_2O_3 and 10.0 wt % CeO_2/3.0 wt % TiO_2-γ-Al_2O_3 has equal number of basic sites appearing at almost the same different temperatures. Both 5.0 wt % NiO/3.0 wt % TiO_2-γ-Al_2O_3 and 10.0 wt % CeO_2/3.0 wt % TiO_2-γ-Al_2O_3 have three basic sites with one of these sites having high and strong basicity centered at a temperature around 310°C.

For the peaks appearing at the different temperature ranges, peaks in the temperature range 50–125°C correspond to weak basic sites, peaks at 160–185°C fall under the category of intermediate strength basic sites, while the peaks at 260°C correspond to strong basicity site. An elbow peak was observed for all of the samples, except for 5.0 wt % NiO/3.0 wt % TiO_2-γ-Al_2O_3 and 10.0 wt % CeO_2/3.0 wt %TiO_2-γ-Al_2O_3, at temperature centered around 500°C. This peak had no significant CO_2 uptake.

Preprints (www.preprints.org) | NOT PEER-REVIEWED | Posted: 18 December 2018 doi:10.20944/preprints201812.0215.v1

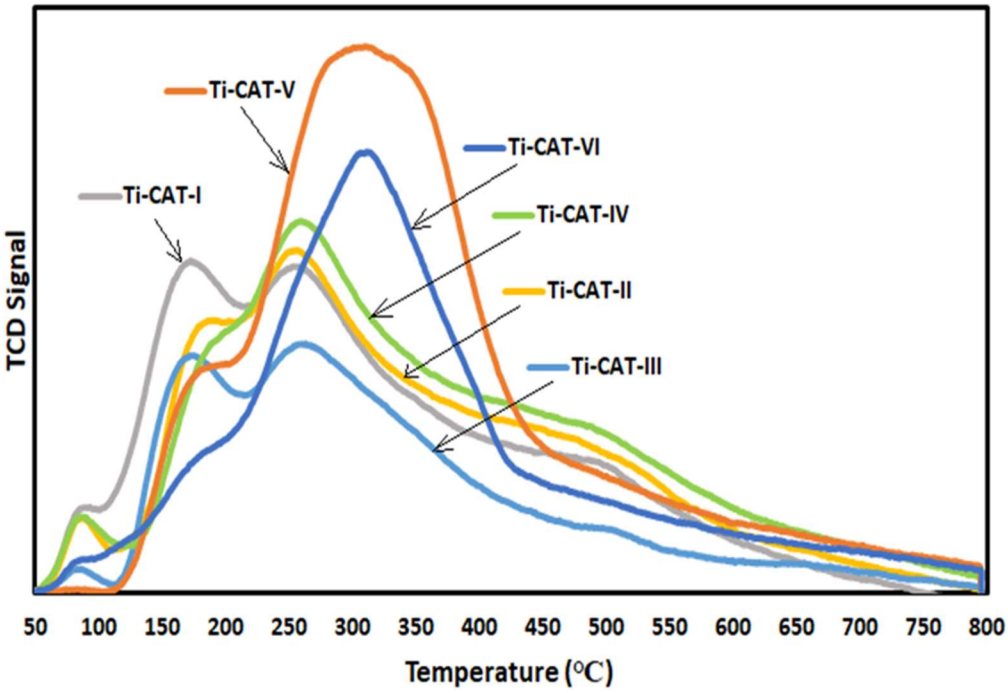

Figure 3: CO_2-TPD profiles of the synthesized catalysts

2.4. Surface Characterization

The textural properties of the fresh catalysts were studied using nitrogen adsorption-desorption isotherms. The results obtained from the N_2 physisorption are shown in Table 2 and that of the isotherms are presented in Figure 4. The results give an insight of the variations in the activities of the catalysts. In accordance to IUPAC classifications of isotherms, the isotherms in Figure 4 fall under the category of type IV with H3-type hysteresis loop which results from capillary condensation and evaporation at high relative pressures [31].

Preprints (www.preprints.org) | NOT PEER-REVIEWED | Posted: 18 December 2018 doi:10.20944/preprints201812.0215.v1

Table 2: N_2 physisorption results for the different catalysts

Catalyst	BET surface area (m^2/g)	Av. Pore diameter (Å)	Pore volume (cm^3/g)
Ti-CAT-I	284.18	115.08	0.40
Ti-CAT-II	283.43	124.45	0.43
Ti-CAT-III	326.20	117.59	0.43
Ti-CAT-IV	256.21	123.00	0.39
Ti-CAT-V	333.83	123.89	0.43
Ti-CAT-VI	299.17	125.19	0.40

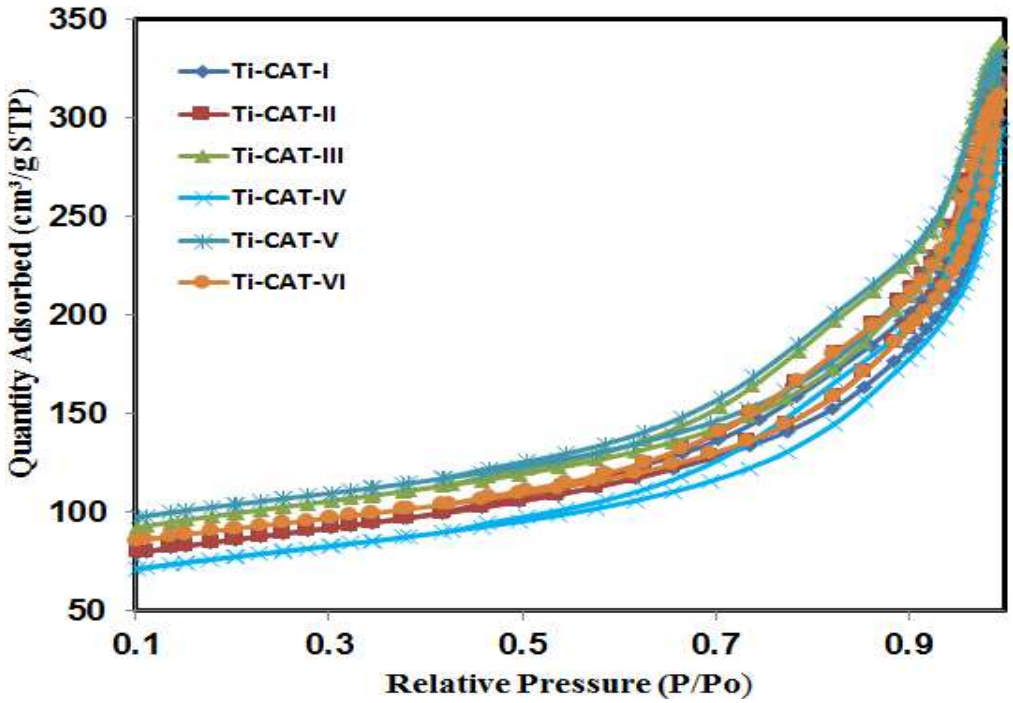

Figure 4: N_2 adsorption-desorption isotherms for Ti-CAT samples

The effect of surface area variation was observed when Mg, Ce and Ni were combined. Table 2 shows that the surface area of the combined metal catalysts reduced relative to single-metal catalysts. This observation is because of the combined metal deposition on the porous structure of the support and filling its pores [32].

Preprints (www.preprints.org) | NOT PEER-REVIEWED | Posted: 18 December 2018 doi:10.20944/preprints201812.0215.v1

2.5. H_2-TPR and TG Analysis

The reduction behavior of the different catalyst samples was investigated using H_2-TPR and the profiles are presented in figure 5(A). The nickel reduction peaks for Ti-CAT-x (x= I, II, III), samples containing Ni combined with other metals, are characterized by three reduction regions at low, medium and high temperature ranges, which are dependent on the degree of dispersion and interaction of the active metal with the support. From these results, the nickel phase reducibility was influenced by the combination of the metals. The reduction peak in the temperature range of 280-380°C could be assigned to the reduced species of NiO having weak interaction with the support, while the peaks that appeared in the temperature range of 600-700°C might be linked to the reduction of NiO species having strong interaction with the support, and a reduction peak of Ni^{2+}-derived from spinel could be found at around 810°C [33].

For Ti-CAT-V i.e. the catalyst with only Ni, the NiO reduction peaks appeared narrower, more intense in temperature ranges lower than those of combined metal counterparts.

Only two reduction peaks were noticeable for Ti-CAT-VI (10.0 wt % CeO_2/3.0 wt % TiO_2–γ-Al_2O_3) at temperature ranges centered at 260 and 325°C. Similar reduction peaks are expected for CeO_2 promoted samples but they appeared to have merged with the peaks for NiO that appeared around that temperature range.

At the end of the reaction that lasted for seven hours, the used catalysts were subjected to TGA, a quantitative analysis that determines the amount of carbon deposition. Figure 5(B) shows the result of the analysis. Catalysts, which showed no sign of reaction, were exempted from this analysis. The weight% loss for virtually all the catalysts began at around 620°C. The TGA profiles revealed that both Ti-CAT-V and MgO-promoted catalysts had the lowest weight loss of about 15.0% carbon deposition, while the two most reactive catalysts (Ti-CAT-II and Ti-CAT-I) had the highest amount of carbon deposition of about 25.0 wt %.

From this result, it can be inferred that the combined metal catalysts, namely Ti-CAT-II and Ti-CAT-I, only enhanced the feed conversion capacity of the catalysts and had less effect in retarding carbon deposition.

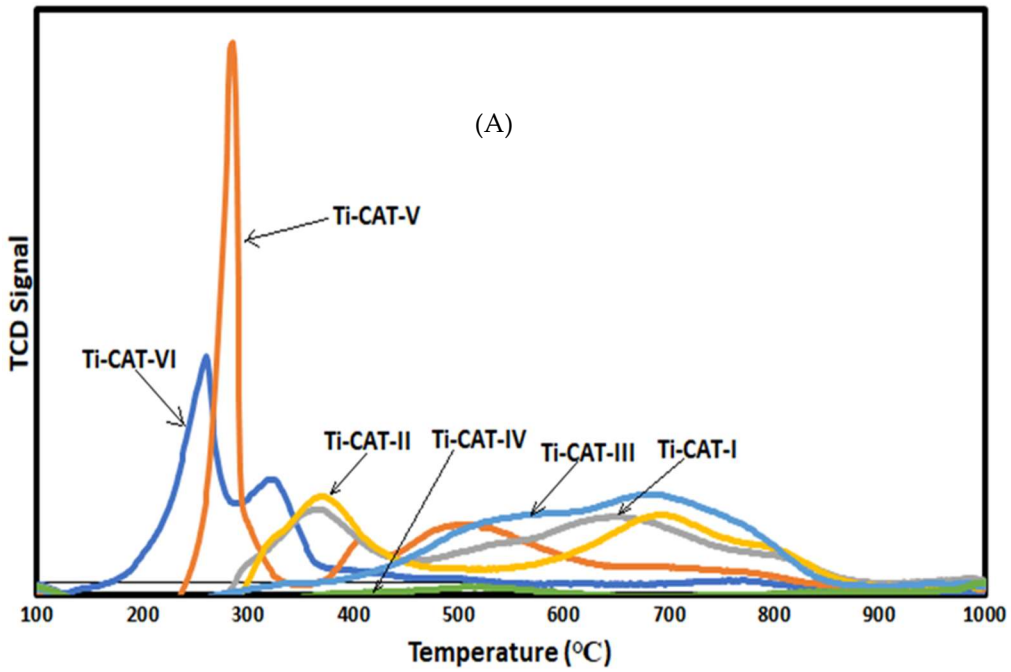

Preprints (www.preprints.org) | NOT PEER-REVIEWED | Posted: 18 December 2018 doi:10.20944/preprints201812.0215.v1

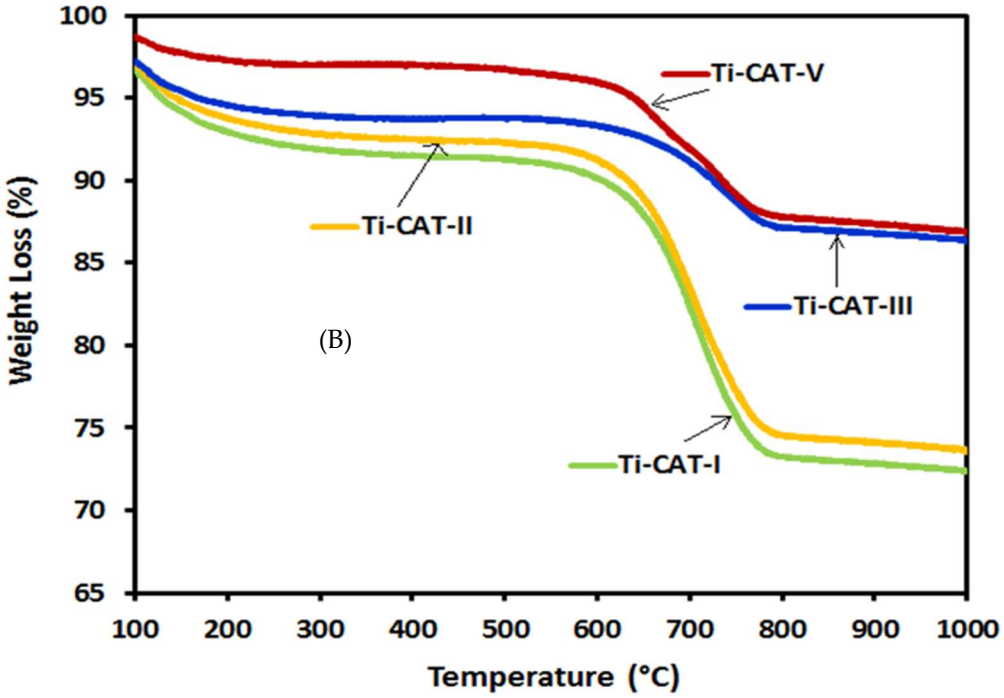

Figure 5: (A) TPR profiles of the promoted and un-promoted catalysts (B) TGA profiles for the spent catalysts

2.6. Effect of Mg and Ce combination on the catalytic performance

The effect of combining CeO_2 and MgO on Ti-CAT-V and their catalytic performance were studied by comparing the activities of Ti-CAT-V catalyst with the those of Ti-CAT-I, Ti-CAT-II, and Ti-CAT-III. CH_4, CO_2 conversions and H_2/CO mole ratio at temperature of 700°C, for 7.0 hours' time-on-stream for DRM, were calculated and plotted as shown in Figure 6(A), (B) and (C). All the combined catalysts have CH_4 and CO_2 conversions higher than that of the 5%Ni/3TiO_2-γ-Al_2O_3 catalyst except for Ti-CAT-VI and Ti-CAT-IV which showed no sign of reaction during the DRM. Ti-CAT-II had the highest CH_4 conversion of about 55% at the start of the reaction and maintained stability at around 52%. The high specific surface area of the catalyst (283.43 m^2/g) enhanced the adsorption, diffusion and contact of the reactant gases which were of great benefit to its catalytic performance. The high average pore diameter and pore volume of Ti-CAT-II may also be another reason for its best performance.

The same trend was observed for CO_2 conversion with the Ti-Cat-V catalyst having the least conversion. For all the catalysts under investigation, CO_2 conversion was observed to be higher than CH_4 conversion which is suggestive of the occurrence of reverse water gas shift (RWGS) reaction. Wang et al. gave the same observation in their study on catalytic hydrogenation of carbon dioxide [34].

$$H_2 + CO_2 \rightarrow CO + H_2O \qquad \Delta H_{298} = +41.2\ \text{kj/mol}$$

In addition, the H_2/CO mole ratio of values less than 1, for all the catalysts, confirmed the occurrence of RWGS as a side reaction.

Preprints (www.preprints.org) | NOT PEER-REVIEWED | Posted: 18 December 2018 doi:10.20944/preprints201812.0215.v1

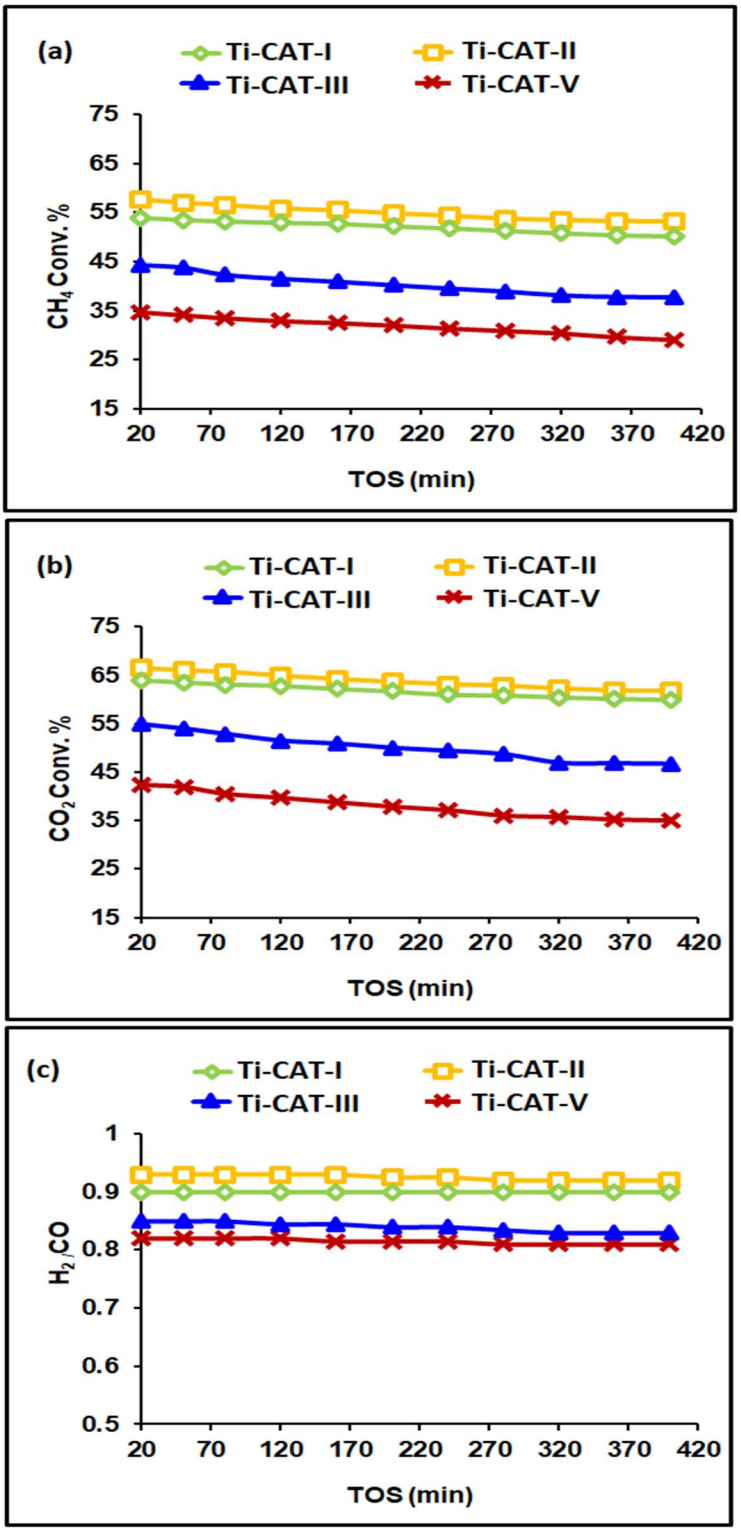

Figure 6: Catalytic performance of Ti-CAT-I, Ti-CAT-II, Ti-CAT-III, and Ti-CAT-V (A) CH_4 conversion (B) CO_2 conversion and (C) H_2/CO ratio

Preprints (www.preprints.org) | NOT PEER-REVIEWED | Posted: 18 December 2018 doi:10.20944/preprints201812.0215.v1

Ti-CAT-II catalyst resulted in a H_2/CO mole ratio value closest to 1 than any of the tested catalysts. The desirable value of the syngas ratio suitable for downstream Fischer-Tropsch synthesis of valuable chemicals is one [35], thus making it the best option for the dry reforming.

2.7. Effect of space velocity

The effect of gas hourly space velocity (GHSV) was studied on the catalyst that showed the best performance in the previous section (i.e. Ti-CAT-II catalyst). GHSV of 19,500 and 78,000 $\frac{\text{feed flow rate}}{\text{mass of cat.}}\left(\frac{\text{ml}}{\text{g.hr}}\right)$ were considered at 700°C and time on stream over 7.0 hours for DRM, while keeping the mass of the catalyst constant. These GHSV values were as half and twice as of the initial GHSV of 39,000 (ml g^{-1} hr^{-1}) respectively. The results in terms of CO_2 and CH_4 conversions as well as H_2/CO mole ratio were calculated and plotted in figures 7(A) and (B). As the GHSV increased, the CH_4 and CO_2 conversions decreased with the highest conversions for both CH_4 and CO_2 obtained at GHSV of 19,500 $\frac{\text{feed flow rate}}{\text{mass of cat.}}\left(\frac{\text{ml}}{\text{g.hr}}\right)$. The decrease in conversions can be attributed to the feed having less residence time at higher GHSV [36]. A similar trend was observed with H_2/CO mole ratio, where it decreased from a ratio of 1 to around 0.8. However, the results at GHSV of 39,000 were the most stable in comparison to those obtained at the other GHSV values.

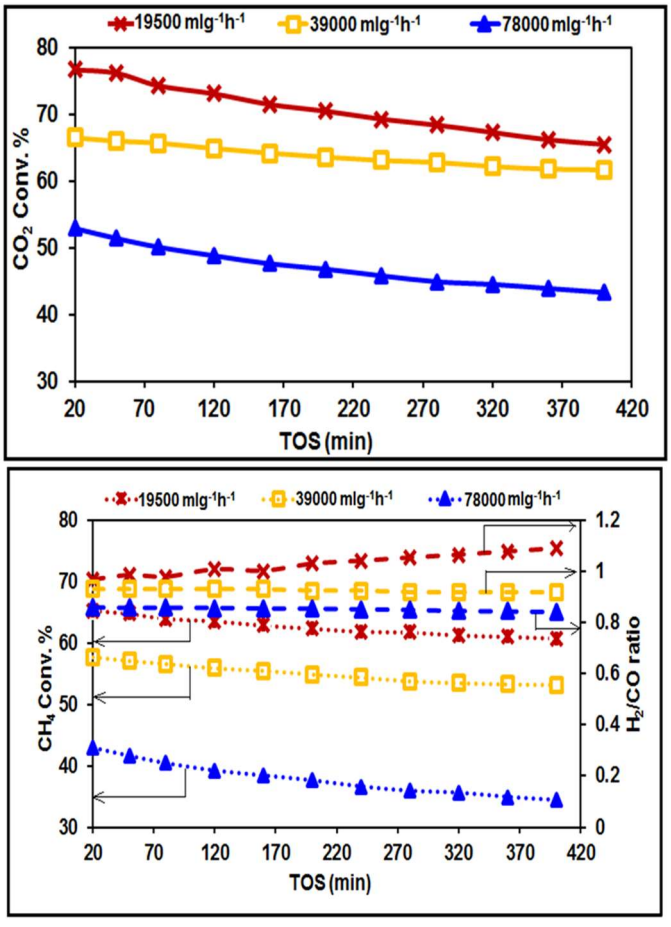

Figure 7: (A) CO_2 conversion for Ti-CAT-II at different gas hourly space velocity (B) CH_4 and H_2/CO ratio for Ti-CAT-II catalyst at different space velocity

Preprints (www.preprints.org) | NOT PEER-REVIEWED | Posted: 18 December 2018 doi:10.20944/preprints201812.0215.v1

2.8. Effect of GHSV on Carbon Deposition

Quantitative analysis of carbon deposition was performed on the catalyst Ti-CAT-II used in methane dry reforming at 3 different space velocities 19,500, 39,000 and 78,000 (ml g^{-1} hr^{-1}).

The results obtained after the completion of the reactions are shown in figure 8. The analysis for the reaction performed at 19500 ml/(g.h) showed the least amount of carbon deposition of about 18%, proving that the DRM took place and not thermal decomposition at this GHSV. The reactions carried out at 39,000 and 78,000 ml/(g.h) showed relatively higher carbon deposition of about 26 and 25%, respectively, indicating that the catalyst had little effect on methane conversion due to the lack of much contact time at these GHSV values and the conversion was mostly by thermal decomposition.

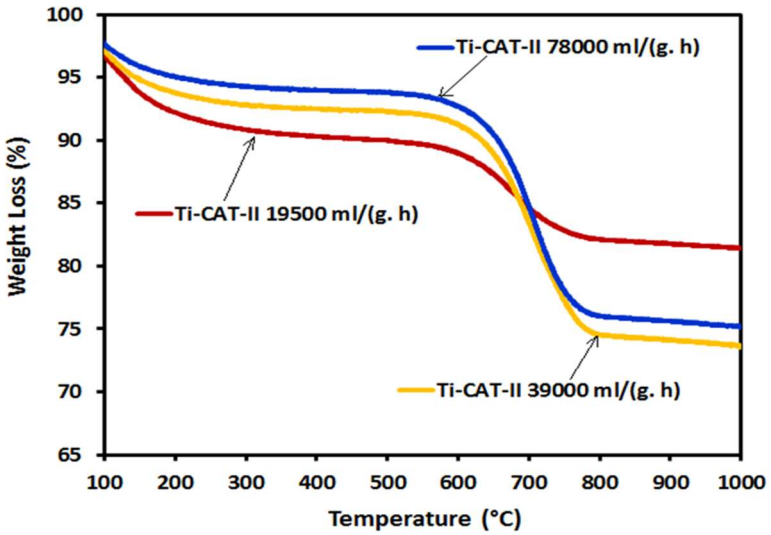

Figure 8: TGA curves for Ti-Cat-II at 19,500, 39,000 and 78,000 ml/ (g.h) GHSV values.

2.9. Effect of different CO_2/CH_4 ratios

The mole ratio of CO_2 to CH_4 was varied at a fixed total flow rate to study the performance of Ti-CAT-II catalyst when CH_4 was supposed to act as the limiting reagent in excess of CO_2 at 700°C and 39,000 ml/(g. h) GHSV. The results are shown in figure 9 (a), (b) and (c). The highest CH_4 conversion of about 78% was obtained when CO_2 was in 20% excess of CH_4, while the least conversion of CH_4 ≅ 43% resulted when the amount of CO_2 was 50% of the required stoichiometric amount in the feed. This observation was expected as CH_4 would have enough CO_2 to undergo dry reforming. On the other hand, the highest CO_2 conversion of ≅ 90% was observed when CO_2 was the limiting reagent. This observation could be due to excess CH_4 present in the feed. The CO_2 conversion reduced with the reaction time-on-stream. Such observation could be ascribed to the disproportionation of carbon monoxide into CO_2 and graphite, a transformation known as Boudouard reaction:

$2CO(g) = CO_{2(g)} + C_{(s)}$

Comparing the different CO_2/CH_4 ratios, it was observed that CH_4 conversion increased with the ratio up to 1.2 (i.e. 0.5<1.0<1.2) and then declined slightly at 1.5. however, the conversion for CO_2 was seen to be decreasing as the ratio was increased (i.e. 1.5<1.2<1.0<0.5).

Preprints (www.preprints.org) | NOT PEER-REVIEWED | Posted: 18 December 2018 doi:10.20944/preprints201812.0215.v1

Figure 9(c) displays the H_2/CO mole ratio results. It was observed that at the lowest CO_2/CH_4 mole ratio, the H_2/CO mole ratio was more than one. This observation could be owing to the insufficient amount of CO_2 for complete dry reforming of the available CH_4 and to the thermal decomposition of unreformed CH_4, giving more H_2 than the stoichiometric amount. Moreover, the Boudouard reaction might contribute to the increase of hydrogen production because the formed CO_2 from Boudouard reaction would shift the DRM equilibrium to the right side.

On the other hand, H_2/CO mole ratio was close to one of the cases where CO_2 was in excess of CH_4, where it was noticed that the H_2/CO mole ratio increased with the reaction time-on-stream. Once again, the Boudouard reaction might be responsible for such observation.

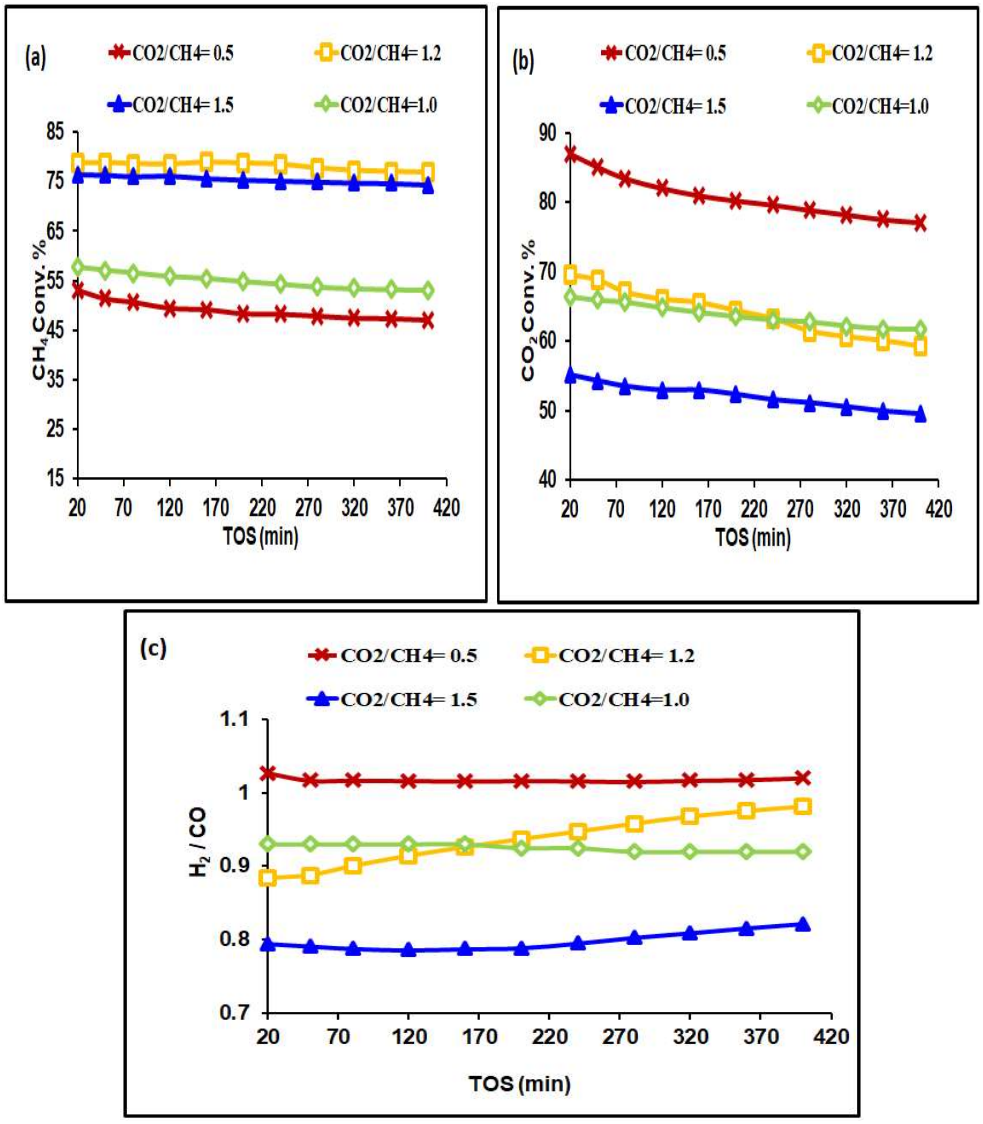

Figure 9: (a) CH_4 (b) CO_2 conversions and (c) H_2/CO ratio for different CO_2/CH_4 ratio

Preprints (www.preprints.org) | NOT PEER-REVIEWED | Posted: 18 December 2018 doi:10.20944/preprints201812.0215.v1

3. Experimental Section

3.1. Materials

Nickel nitrate hexahydrate [$Ni(NO_3)_2.6H_2O$, 98%, Alfa Aesar], cerium nitrate hexahydrate [$Ce(NO_3)_3.6H_2O$, 99.0% assay on Ce basis, general purpose reagent, BDH], magnesium acetate tetra-hydrate [$Mg(O_2CCH_3)_2.4H_2O$, 99.5-102.0%, Merck] were commercially available and were used without further purification. γ-Alumina doped with titania (3.0 wt % TiO_2/γ-Al_2O_3) in the shape of pellets, was a gift from Dr. Tiancun Xiao, Senior Research Fellow, Inorganic Chemistry Laboratory, Oxford University. Ultrapure deionized water (18.2 MΩ.cm) was obtained from a Milli-Q water purification system (Millipore).

3.2. Catalyst Preparation

The required amounts of $Ni(NO_3)_2.6H_2O$, Ce $(NO_3)_3{\cdot}6H_2O$, Mg $(O_2CCH_3)_2{\cdot}4H_2O$, and support were mixed and were ground together to fine powder by pestle and mortar. Small amount of ultrapure water was used to convert the solid mixture into a paste, which was spun mechanically until dryness. The paste and spinning process was repeated three times. The final solid was calcined in a digital, programed muffle furnace at 600°C for three hours by ramping temperature from room temperature by a rate of 3.0°C/minute. The denotation of the prepared catalyst samples and their wt % loadings of nickel oxide, ceria, and magnesia at 600°C calcination are given below in Table 3.

Table 3: Prepared catalyst samples and the wt % of their composition

Catalyst	Concentration, wt %		
	NiO	CeO_2	MgO
Ti-CAT-I	5.0	10.0	1.0
Ti-CAT-II	5.0	10.0	0.0
Ti-CAT-III	5.0	0.0	1.0
Ti-CAT-IV	0.0	10.0	1.0
Ti-CAT-V	5.0	0.0	0.0
Ti-CAT-VI	0.0	10.0	0.0

3.3. Catalyst Characterization

The metallic component composition of all catalysts was determined by an Agilent 7800 inductively-coupled plasma mass spectrometry (ICP) at the laboratory of IDAC Merieux NutriSciences, Riyadh, Saudi Arabia. Carbon deposition on the used catalysts was measured by thermogravimetric analysis (TGA) under air by using a Shimadzu TGA-51. A certain amount from the spent catalyst (10 mg) was subjected to heat treatment within the temperature range 25°C-1000°C. Ramping temperature was maintained at 20°C/min. The Brunauer-Emmet-Teller technique was adopted in calculating the surface area per unit mass of the samples using a device

Preprints (www.preprints.org) | NOT PEER-REVIEWED | Posted: 18 December 2018 doi:10.20944/preprints201812.0215.v1

that analyses surface area and porosity i.e. Micromeritics Tristar II 3020. For nitrogen physisorption measurements, an amount of 0.20–0.30 g weighed from the catalyst was subjected to degassing at 300°C for three hours prior to analysis. The reducibility of the fresh catalysts was determined by the Micromeritics AutoChem II. A sample weight of 75.0 mg was analyzed. Samples were first heated under argon (99.9%) at 150°C for 30 min, thereafter cooled to 25°C. Afterwards, samples were heated to 1000°C at 10°C/min by allowing the flow of 10% H_2/Ar gas at 40 ml/min. A thermal conductivity detector (TCD) was used to follow the H_2 consumption. Temperature programmed desorption of carbon dioxide (CO_2-TPD) and CO pulse chemisorption measurements were obtained from an automatic chemisorption equipment (Micromeritics AutoChem II 2920) with a TCD. At the start a 70 mg sample was heated at 200°C for 1 h under helium (He) flow to remove adsorbed components. Then, CO_2 adsorption was carried out at 50°C for 60 min in the flow of He/CO_2 gas mixture (90/10 L/L) with a flow rate of 30.0 ml/min. Afterward, a linear temperature rise at a rate of 10°C/min until 800°C was registered by the TCD of CO_2 desorption signal. X-ray powder diffraction patterns for the samples were recorded on a Bruker D8 Advance XRD diffractometer by using Cu K_α radiation source and a nickel filter, operated at 40 kV and 40 mA. The step size and scanning range of 2θ for analysis was set to 0.01° and 5–100°, respectively. The present phases were documented using standard powder XRD cards (JCPDS). Catalysts' morphology was studied using JEOL JSM-7100F field emission scanning electron microscope, equipped with energy-dispersive X-ray spectroscopy (EDXS) for surface elemental analysis.

3.4. Catalystic Perfromance

Methane reforming reaction was accomplished in a fixed-bed tubular stainless steel micro-reactor (ID = 9 mm) at atmospheric pressure. The reactor system was provided by process integral development (PID Eng. & Tech). Before performing the DRM reaction, a 0.10 g catalyst was activated by H_2 flow of 40 ml/min at 700 °C for 60 minutes. N_2 gas was then admitted to the reactor for 20 min to remove adsorbed H_2 while the catalyst was kept at reaction temperature (700°C). Afterwards, feed gases of CH_4, CO_2, and N_2 were injected at flow rates of 35, 35 and 5 ml/min, respectively. The temperature, pressure and reaction variables were inspected through the reactor panel. A GC (GC-2014 SHIMADZU) unit having a thermal conductivity detector and two columns, Porapak Q and Molecular Sieve 5A, was connected in series/bypass connections in order to have a complete analysis of the reaction products. The following equations were used to calculate the CH_4 and CO_2 conversions respectively.

$$\%CH_4 \text{ conversion} = \frac{CH_4 \text{ in} - CH_4 \text{ out}}{CH_4 \text{ in}} \text{ X } 100$$

$$\%CO_2 \text{ conversion} = \frac{CO_2 \text{ in} - CO_2 \text{ out}}{CO_2 \text{ in}} \text{ X } 100$$

4. Conclusions

This paper investigated the dry reforming of methane, CH_4, over 5.0 wt % NiO/3.0 wt % TiO_2+γ-Al_2O_3 catalyst, Ti-CAT-V, and the effects of promoters such as CeO_2 and MgO, on the catalytic activity and stability of the catalyst. The promoter loading was 10.0 wt % and 1.0 wt % for CeO_2 and MgO respectively. Promoted Ti-CAT-V catalyst showed better conversion of both CH_4 and CO_2 than the un-promoted counterpart. 5.0 wt % Ni.O-10.0 wt % CeO_2/3.0 wt % TiO_2+γ-Al_2O_3 had the highest CH_4 and CO_2 conversion of about 55% and 64% respectively, while no reaction was observed for 10.0 wt %CeO_2/3.0 wt% TiO_2+γ-Al_2O_3 and 10.0 wt % CeO_2+1.0 wt % MgO/3.0 wt %

 doi:10.20944/preprints201812.0215.v1

TiO_2+γ-Al_2O_3. It can be inferred from the improved performance of the promoted catalysts that the promoters had a positive influence on the textural properties, metal support interaction and reduction behaviour of the catalyst. These impacts of promoters were well shown by the used characterization techniques used. From the thermogravimetric analysis, un-promoted catalyst gave the lowest carbon deposition. This result implied that the promoters only enhanced the performance of the catalyst and had less effect in retarding carbon deposition relative to the un-promoted catalyst.

Ti-CAT-V was selected for further investigation at different GHSVs and subsequently at various CO_2/CH_4 ratios. An inverse relationship between GHSV and catalytic activity was observed. A GHSV of 19500 $\frac{\text{feed flow rate}}{\text{mass of cat.}}\left(\frac{\text{ml}}{\text{g.hr}}\right)$ and CO_2/CH_4 ratio of 0.5 gave the best results.

Author Contributions: A.S.F., A.H.F, S.O.K., R.Ar., R.As. and A.B. carried out all experiments and characterization tests as well as shared in the analysis of the data and shared in the writing of the manuscript. A.S.F, S.O.K, A.E.A and A.B. wrote the paper and shared data analysis. A.H.F and A.A.I. contributed in writing the paper and edited it.

Funding: This research was funded by the Deanship of Scientific Research at King Saud University, Project No. RGP-1435-078.

Acknowledgments: The authors would like to express their sincere appreciation to the Deanship of Scientific Research at King Saud University for its funding for this research group project No. (RG-1435-078)

Conflicts of Interest: The authors declare no conflict of interest.

References

1. Albarazi, A.; Beaunier, P.; Da Costa, P. Hydrogen and syngas production by methane dry reforming on SBA-15 supported nickel catalysts: On the effect of promotion by Ce0.75Zr0.25O_2 mixed oxide. *Int. J. Hydrog. Energy* **2013**, 38, 127-139.
2. Bao, Z.; Lu, Y.; Han, J.; Li, Y.; Yu, F. Highly active and stable Ni based bimodal pore catalysts for dry reforming of methane. *Appl. Catal. A Gen.* **2015**, 491, 116-126.
3. Buelens, L.C.; Galvita, V.V.; Poelman, H.; Detavernier, C.; Marin, G.B. Super-dry reforming of methane intensifies CO_2 utilization via Le Chatelier's principle. *Science* **2016**, 354, 449-452.
4. Julián-Durán, L.M.; Ortiz-Espinoza, A.P.; El-Halwagi, M.M.; Jiménez-Gutiérrez, A. *ACS Sustain. Chem. Eng.* **2014**, *2*, 2338–2344.
5. Schulz, H. Short history and present trends of Fischer-Tropsch synthesis. *Appl. Catal. A Gen.* **1999**, 186, 3-12.
6. Sheu, E.J.; Mokheimer, E.M.A.; Ghoniem, A.F. A review of solar methane reforming systems. *Int. J. Hydrog. Energy* **2015,** 40, 12929–12955.
7. Barelli, L.; Bidini, G.; Gallorini, F.; Servili, S. Hydrogen production through sorption-enhanced steam methane reforming and membrane technology. *Energy* **2008**, 33, 554–570.
8. Hyunjin, Ji.; Junghun, L.; Eunyeong, C.; Ilsung, S. Hydrogen production from steam reforming using an indirect heating method. *Int. J. Hydrog. Energy* **2018**, 43, 3655-3663.
9. Cyril, P.; Wenhao, F.; Mickaël, C.; Sébastien, P.; Louise, J.D. Steam reforming, partial oxidation and oxidative steam reforming for hydrogen production from ethanol over cerium nickel based oxyhydride catalyst. *Appl. Catal. A Gen.* **2016**, 518, 78-86.
10. Yousri, M.A.W.; Mohamed, M.E.G.; Nader, R.A. Steam and partial oxidation reforming options for hydrogen production from fossil fuels for PEM fuel cells. *AEJ* **2012**, 51, 69-75.
11. Devin, M.W.; Sandra, L.P.; John, T.W.; John, N.K. Synthesis gas production to desired hydrogen to carbon monoxide ratios by tri-reforming of methane using Ni–MgO–(Ce,Zr)O_2 catalysts. *Appl. Catal. A Gen.* **2012**, 445–446, 61-68.

12. Linus, A.S.; Lea, C.S.K.; Karla, H.D.; Stephan, A.S.; Johannes, A. L. On the coke deposition in dry reforming of methane at elevated pressures. *Appl. Catal. A Gen*. **2015**, 504, 599-607.
13. Drif, A.; Bion, N.; Brahmi, R.; Ojala, S.; Pirault-Roy, L.; Turpeinen, E.; Seelam, P.K; Keiski, R.L.; Epron, F. Study of the dry reforming of methane and ethanol using Rh catalysts supported on doped alumina. *Appl. Catal. A Gen*. **2015,** 504, 576-584.
14. Jabbour, K.; El Hassan, N.; Casale, S.; Estephane, J.; El Zakhem, H. Promotional effect of Ru on the activity and stability of Co/SBA-15 catalysts in dry reforming of methane. *Int. J. Hydrog. Energy* **2014,** 39, 7780-7787.
15. Du, X.; France, L. J.; Kuznetsov, V. L.; Xiao, T.; Edwards, P. P.; AlMegren, H.; Bagabas, A. Dry Reforming of Methane Over ZrO_2-Supported Co–Mo Carbide Catalyst. *Appl. Petrochem. Res.* **2014**, 4, 137-144.
16. France, L.J.; Du, X.; Almuqati, N.; Kuznetzov, V.L.; Zhao, Y.; Zheng, J.; Xiao, T.; Bagabas, A.; Almegren, H.; Edwards, P.P. The Effect of Lanthanum Addition on The Catalytic Activity of γ-Alumina Supported Bimetallic Co–Mo Carbides for Dry Methane Reforming. *Appl. Petrochem. Res.* **2014**, 4, 145-156.
17. Tao, X.; Wang, G.; Huang, L.; Li, X.; Ye, Q. Effect of Cu-Mo Activities on the NiCuMo/Al_2O_3 Catalyst for CO_2 Reforming of methane. *Catal. Lett.* **2016,** 146, 2129-2138.
18. Budiman, A.W.; Song, S.-H.; Chang, T.-S.; Shin, C.-H.; Choi, M.-J. Dry reforming of methane over cobalt catalysts: a literature review of catalyst development. *Catal. Surv. Asia* **2012,** 16, 183-197.
19. Park, J.H.; Lee, D.; Lee, H.C.; Park, E.D. Steam reforming of liquid petroleum gas over Mn-promoted Ni/γ-Al_2O_3 catalysts. *Korean J. Chem. Eng.* **2010**, 27, 1132–1138.
20. Gao, X.; Bare, S.R.; Fierro, J.L.G.; Banares, M.A.; Wachs, I.E. Preparation and in-Situ Spectroscopic Characterization of Molecularly Dispersed Titanium Oxide on Silica. *J. Phys. Chem. B* **1998**, 102, 5653–5666.
21. Klein, S.; Thorimbert, S.; Maier, W.F. Amorphous microporous titania–silica mixed oxides: preparation, characterization, and catalytic redox properties. *J. Catal.* **1996,** 163, 476–488.
22. Miller, J.B.; Ko, E.I. Control of mixed oxide textural and acidic properties by the sol-gel method. *Catal. Today* **1997,** 35, 269-292.
23. Niu, F.; Li, S.; Zong, Y.; Yao, Q. Catalytic Behavior of Flame-Made Pd/TiO_2 Nanoparticles in Methane Oxidation at Low Temperatures. *J. Phys. Chem. C* **2014,** 118, 19165–19171.
24. Tauster, S.J.; Fung, S.C.; Baker, R.T.K.; Horsely, J.A. Partial Oxidation of Methane to Synthesis Gas over Ru/TiO_2 Catalysts: Effects of Modification of the Support on Oxidation State and Catalytic Performance. *Science*, **1981,** 211, 1121-1125.
25. Shamskar, F.R.; Meshkani, F.; Rezaei, M. Preparation and characterization of ultrasound-assisted co-precipitated nanocrystalline La-, Ce-, Zr –promoted Ni-Al_2O_3 catalysts for dry reforming reaction. *J. CO_2 Util.* **2017**, 22, 124-134.
26. Jang, W.J.; Jung, Y.S.; Shim, J.O.; Roh, H.S.; Yoon, W.L. Preparation of a Ni-MgO-Al_2O_3 catalyst with high activity and resistance to potassium poisoning during direct internal reforming of methane in molten carbonate fuel cells. *J. Power Sources* **2018,** 378, 597-602.
27. Ahmed, S.A.A.; Anis, H.F.; Ahmed, E.A. Effects of Selected Promoters on Ni/Y-Al_2O_3 Catalyst Performance in Methane Dry Reforming. *Chinese J. Catal.* **2011,** 32, 1604-1609.
28. Zhu, F.; Zhang, H.; Yan, X.; Yan, J.; Ni, M.; Li, X.; Tu, X. Plasma-catalytic reforming of CO_2-rich biogas over Ni/γ-Al_2O_3 catalysts in a rotating gliding arc reactor. *Fuel* **2017,** 199, 430–437.
29. Mei, D.; Ashford, B.; He, Y.-L.; Tu, X. Plasma-catalytic reforming of biogas over supported Ni catalysts in a dielectric barrier discharge reactor: effect of catalyst supports. *Plasma Process. Polym.* **2017,** 14, 1600076.
30. Akbari, E.; Alavi, S.M.; Rezaei, M. Synthesis gas production over highly active and stable nanostructured NiMgOAl_2O_3 catalysts in dry reforming of methane: effects of Ni contents. *Fuel* **2017,** 194, 171 – 179.
31. Sudarsanam, P.; Hillary, B.; Deepa, D.K.; Amin, M.H.; Mallesham, B.; Reddy, B.M.; Bhargava, S.K. Highly efficient cerium dioxide nanocube-based catalysts for low temperature diesel soot oxidation: the cooperative effect of cerium- and cobalt-oxides. *Catal. Sci. Technol.* **2015,** 5, 3496–3500.

 doi:10.20944/preprints201812.0215.v1

32. Pudukudy, M.; Yaakob, Z.; Akmal, Z.S. Direct decomposition of methane over SBA-15 supported Ni, Co and Fe based bimetallic catalysts. *Appl. Surf. Sci.* **2015,** 330, 418–430.
33. Siew, K.W.; Lee, H.C.; Gimbun, J.; Chin, S.Y.; Khan, M.R.; Taufiq-Yap, Y.H.; Cheng, C.K. Syngas production from glycerol-dry (CO2) reforming over La-promoted Ni/ Al_2O_3 catalyst. *Renew. Energy* **2015,** 74, 441–447.
34. Wang, W.; Wang, S.P.; Ma, X.B.; Gong, J.L. Recent advances in catalytic hydrogenation of carbon dioxide. *Chem. Soc. Rev.* **2011**, 40, 3703-27.
35. Wu, J.; Fang, Y.; Wang, Y.; Zhang, D.K. Combined coal gasification and methane reforming for production of syngas in a fluidized-bed reactor. *Energ. Fuel*, **2005,** 19, 512-516.
36. Lalit, S.G.; Guido, S.J.S.; Valero-Romero, M.J.; Mallada, R.; Santamaria, J.; Stankiewicz, A.I.; Stefanidis, G.D. Synthesis, characterization, and application of ruthenium-doped $SrTiO_3$ perovskite catalysts for microwave-assisted methane dry reforming. *Chem. Eng. Process.: Process Intensification* **2018,** 127, 178–190.